applied sciences

MDPI

Article

Electric Field and Temperature Effects on the Ab Initio Spectroscopy of Liquid Methanol

Giuseppe Cassone [1,*], Sebastiano Trusso [1], Jiri Sponer [2] and Franz Saija [1]

[1] Institute for Chemical-Physical Processes, National Research Council of Italy (IPCF-CNR), Viale F. Stagno d'Alcontres 37, 98158 Messina, Italy; trusso@ipcf.cnr.it (S.T.); saija@ipcf.cnr.it (F.S.)
[2] Institute of Biophysics of the Czech Academy of Sciences (IBP-CAS), Královopolská 135, 61265 Brno, Czech Republic; sponer@ncbr.muni.cz
* Correspondence: cassone@ipcf.cnr.it; Tel.: +39-090-3976-2220

Abstract: Although many H-bonded systems have been extensively investigated by means of infrared (IR) spectroscopy, the vibrational response to externally applied electric fields of polar liquids remains poorly investigated. However, local electric fields along with quantum-mechanical interactions rule the behavior of H-bonded samples at the molecular level. Among the many H-bonded systems, liquid methanol holds a key place in that it exhibits a very simple H-bond network where, on average, each molecule acts as a single H-bond donor and, at the same time, as a single H-bond acceptor. Here we report on the IR spectra emerging from a series of state-of-the-art ab initio molecular dynamics simulations of bulk liquid methanol under the action of static and homogeneous electric fields. In addition, the same analysis is here conducted in the absence of the external field and for different temperatures. Although some electric-field-induced effects resemble the response of other polar liquids (such as the global contraction of the IR spectrum upon field exposure), it turns out that, distinctly from water, the "electrofreezing" phenomenon is unlikely to happen in liquid methanol. Finally, we provide atomistic analyses magnifying the completely different nature of electric-field- and temperature-induced effects on bulk liquid methanol and on its vibrational response.

Keywords: H-bonded systems; electric fields; spectroscopy; density functional theory; molecular dynamics; methanol

Citation: Cassone, G.; Trusso, S.; Sponer, J.; Saija, F. Electric Field and Temperature Effects on the Ab Initio Spectroscopy of Liquid Methanol. *Appl. Sci.* **2021**, *11*, 5457. https://doi.org/10.3390/app11125457

Academic Editors: Andrea Perucchi and Fabio Novelli

Received: 11 May 2021
Accepted: 11 June 2021
Published: 12 June 2021

1. Introduction

Owing to the presence of a single hydroxyl (OH) group in their molecular structure, monohydric alcohols are very useful systems for the investigation of crucially relevant intermolecular interactions such as hydrogen bonds (H-bonds). Methanol (CH_3OH) is the smallest organic compound capable of exhibiting and developing H-bonded networks and it is largely employed as an organic solvent in many experimental setups [1,2]. In this way, liquid methanol samples are widely used in industry and in the fields of organic synthesis, biochemistry and biotechnology [3–8]. Moreover, the development of direct methanol fuel cells has led, during the last decades, to a broad and continuously growing interest in the understanding of the microscopic properties of methanol [9].

H-bonds in bulk liquid methanol are distinctly different from those typically observed in liquid water. In fact, because of the presence of the hydrophobic methyl (CH_3) groups, methanol does not give rise to the complexity of the tetrahedral arrangement of the intermolecular interactions present in liquid water. In addition, as the methanol molecule is capable of acting as a donor and, at the same time, as an acceptor of only one H-bond (i.e., each molecule in the bulk is involved in two H-bonds on average), the methanol H-bond network typically gives rise to almost linear structures of interconnected molecules in the liquid phase [10–13]. Furthermore, methanol molecules are known to be less polar than water molecules, hence establishing weaker H-bonds between each other than water molecules do in neat aqueous solutions. All these properties, conferring to it one of the

highest simplicities of the percolated intermolecular interactions, render liquid methanol the perfect test bed for the general and fundamental understanding of the H-bonds' behavior. Among other things, indeed, methanol represents a typical example of associating fluid, which displays short-range and strongly directional attractive interactions.

A plethora of experimental and theoretical studies have ascertained that methanol molecules are bound into linear chains that are sometimes interrupted by the presence of bifurcations [14–23]. Notwithstanding the huge amount of fundamental and applied spectroscopic investigations under disparate thermodynamic conditions and chemical environments, the bulk liquid methanol infrared (IR) spectrum in the presence of static electric fields has not been reported so far. Owing also to the pioneering work performed by Shaik et al. [24,25], which theoretically and computationally predicted a series of fundamental effects produced by static electric fields on single-molecule systems, some studies on methanol clusters under electric fields have been carried out by using density functional theory (DFT) approaches [26–29]. Added to the fact that intense electric fields (on the order of 0.1–1.0 V/Å or even more [30–33]) along with quantum-mechanical interactions constitute the foundation of H-bonds and, ultimately, the existence of H-bonded systems, it is also well-known that the application of strong external electric fields can remarkably affect a wide palette of properties of polar fluids [34–37]. In fact, external electric fields on condensed-phase systems may induce plenty of phenomena, because such fields are able to strongly influence redox- and electron-transfer reactions [38,39], can affect covalent and intermolecular bonds [40–42], and can produce the well-known Stark effect [43], as well as the so-called vibrational Stark effect [44,45] (i.e., the field-induced frequency shift of the molecular vibrations). However, the vibrational Stark effect phenomenon has neither been observed nor investigated in liquid methanol. Finally, although it has been claimed that the "electrofreezing" phenomenon occurs in liquid water by pioneering simulation studies conducted with classical force-field water models [46], more recent and sophisticated DFT-based molecular dynamics investigations revealed that, upon the electric field exposure, the liquid water structure becomes more "ice like" [47]. Such evidence has recently been strongly supported by prolonged force-field molecular dynamics simulations [48]. Such a fascinating process, evidencing some analogies between the application of an external electric field and the decrease in the temperature of the sample, has never been extensively investigated for H-bonded systems other than water.

In the current study, by means of state-of-the-art ab initio molecular dynamics (AIMD) simulations, we report on the IR spectrum of liquid methanol under the action of static and homogeneous electric field intensities up to 0.30 V/Å, a value slightly beneath the field-induced molecular dissociation threshold [49,50]. Moreover, with the aim of comparing electric-field-induced and temperature-induced effects, IR spectra of liquid methanol at different temperatures (from 240 K up to 350 K) are also determined.

2. Materials and Methods

We used the software package CP2K [51,52], based on the Born–Oppenheimer approach, to perform ab initio molecular dynamics (AIMD) simulations of samples of neat liquid methanol under the action of static and homogeneous electric fields applied along a given direction (corresponding to the *z*-axis). Moreover, in the zero-field case, several AIMD simulations have also been carried out at different temperatures. The implementation of an external field in simulation algorithms based on density functional theory (DFT) can be achieved by exploiting the Modern Theory of Polarization and Berry's phases [53–55], whereas when periodic boundary conditions apply—as in the current investigation—implementation of static fields is executed owing to the seminal work by Umari and Pasquarello [56]. The interested reader may refer to [34] for a vast presentation of the most used implementations of electric fields in atomistic simulation codes.

Neat methanol samples contained 50 CH_3OH molecules (i.e., 300 atoms) arranged in a cubic cell with edges equal to 14.99 Å, so as to reproduce the liquid methanol experimental density of 0.79 g·cm^{-3} at room temperature. As anticipated above, in order to minimize

nonphysical surface effects, such a structure was replicated in all spatial directions by adopting periodic boundary conditions. The intensity of the electric field was gradually increased with a step increment of 0.05 V/Å from zero up to a maximum of 0.30 V/Å, the latter value being close to the electric field threshold for molecular dissociation at 300 K [49,50]. Beyond this field intensity, indeed, a plethora of electric-field-induced chemical reactions takes place in liquid methanol [57,58]. Moreover, when evaluating pure temperature-induced effects, four different AIMD simulations were executed at the nominal temperatures of 240, 270, 300, and 350 K. In these zero-field cases we performed dynamics of 50 ps, whereas for each other value of the field intensity, we ran dynamics of 20 ps, thus accumulating a global simulation time equal to 320 ps, whereas a time-step of 0.5 fs has been chosen.

Wavefunctions of the atomic species were expanded in triple-zeta valence plus polarization (TZVP) basis sets with Goedecker–Teter–Hutter pseudopotentials using the GPW method [59]. A plane-wave cutoff of 400 Ry was imposed. Exchange and correlation effects were treated with the Becke–Lee–Yang–Parr (BLYP) [60,61] density functional. Moreover, in order to take into account dispersion interactions, we employed the dispersion-corrected version of BLYP (i.e., BLYP-D3) [62,63]. Adoption of the BLYP-D3 functional has been indicated by the widespread evidence that such a functional, when dispersion corrections are taken into account, offers some of the best adherence to the experimental results related to H-bonded systems like water among the standard generalized gradient approximation (GGA) functionals [64,65]. It is well-known indeed that neglecting dispersion corrections leads to a severely over-structured liquid (see, e.g., [66] and references therein). Although some recent findings have magnified the importance of including nuclear quantum effects (NQEs) in the presence of electric fields [33], the required computational cost for the wide palette of simulations here presented renders impracticable the adoption of sophisticated thermostats mimicking NQEs. More importantly, vibrational spectra determined from path-integral AIMD exhibit many critical issues due to the presence of fictitious vibrations induced by thermostats for reproducing NQEs [67,68]. This way, the dynamics of nuclei were simulated classically within a constant number, volume, and temperature (NVT) ensemble using the Verlet algorithm, whereas the canonical sampling was executed by employing a canonical-sampling-through-velocity-rescaling thermostat [69] set with a time constant equal to 10 fs. H-bonds were identified through the following geometric conditions that should be simultaneously fulfilled [20,23]: (i) $r(\mathrm{O}\cdots\mathrm{H})$ bond distance smaller than 2.6 Å; (ii) $\mathrm{O}\cdots\mathrm{O}$ distance smaller than 3.5 Å; (iii) $\angle\mathrm{HO}\cdots\mathrm{O}$ bond angle smaller than 30°.

Infrared (IR) spectra were determined by means of the software TRAVIS [70,71] from the centers of the maximally localized Wannier functions (MLWFs) [72,73] calculated on the fly during the AIMD simulations. A time-step of 2.5 fs, corresponding to 5 AIMD time-steps, was chosen for the MLWFs evaluation in all the investigated cases with exception of the simulations at 0.25 and 0.30 V/Å, where it was necessary to reduce the evaluation step for the MLWF centers to 0.5 fs (i.e., at each AIMD step). This way, by evaluating the Fourier transform of the autocorrelation functions of the molecular dipole moments for all the simulated systems, IR spectra were determined.

3. Results and Discussion

Density functional theory (DFT) generally produces a series of shifts when evaluating and predicting the frequency of vibration of molecular modes. Nevertheless, it not only represents one of the most advanced and precise theoretical methods to deal with these predictions but is also the only one capable of determining—on firm quantum-mechanical bases—vibrational spectra of condensed-phase systems. In this way, vibrational properties of a plethora of liquids and solids have been reported in the literature by means of DFT-based approaches [74]. In condensed matter, infrared (IR) spectra carry useful information not only on the intramolecular vibrations but also on the existing intermolecular interac-

tions. As a consequence, important properties tightly related to the presence of H-bonds have been investigated by means of IR absorption experiments [75,76].

As shown in Figure 1, where the computational and experimental IR spectra are plotted together, all the important vibrational modes characterizing the experimental liquid methanol IR spectrum at room temperature are qualitatively caught by ab initio molecular dynamics (AIMD) simulations. As anticipated, however, significant frequency shifts are detected for almost all the allowed molecular vibrations. As an example, the OH-stretching band, whose center of frequency experimentally falls at about 3350–3400 cm^{-1} [75,77], is found at about 3250–3300 cm^{-1} in our AIMD simulations. However, the CH-stretching band, which is experimentally found at 2800–3000 cm^{-1} [75,78], is localized at 3000 cm^{-1} by the BLYP-D3 exchange and correlation functional used in the current AIMD simulations. Somehow surprisingly, hence, nuclear quantum effects (NQEs), believed to be important for the realistic description of the behavior of light atoms such as hydrogen, seem to only moderately affect the vibrational properties of the symmetric and asymmetric stretching of the methyl groups in liquid methanol at room temperature. In fact, the vibrational band ascribed to the CH_3 bending is also centered around 1400 cm^{-1} both from laboratory experiments [75,76] and from the first-principles molecular dynamics simulations presented here, as shown in Figure 1. Moreover, the typical frequency of vibration of the rocking mode of the methyl groups found in the simulations is in fairly good agreement with the available experimental data (i.e., ∼1100 cm^{-1}). Finally, the low-frequency modes associated with the CO stretching and with the out-of-plane OH bending—experimentally localized around 1000 cm^{-1} and 700 cm^{-1}, respectively—are qualitatively well reproduced by the current room-temperature AIMD simulation, in that they appear only slightly red-shifted and blue-shifted, respectively, by about 100 cm^{-1} each, as displayed in Figure 1.

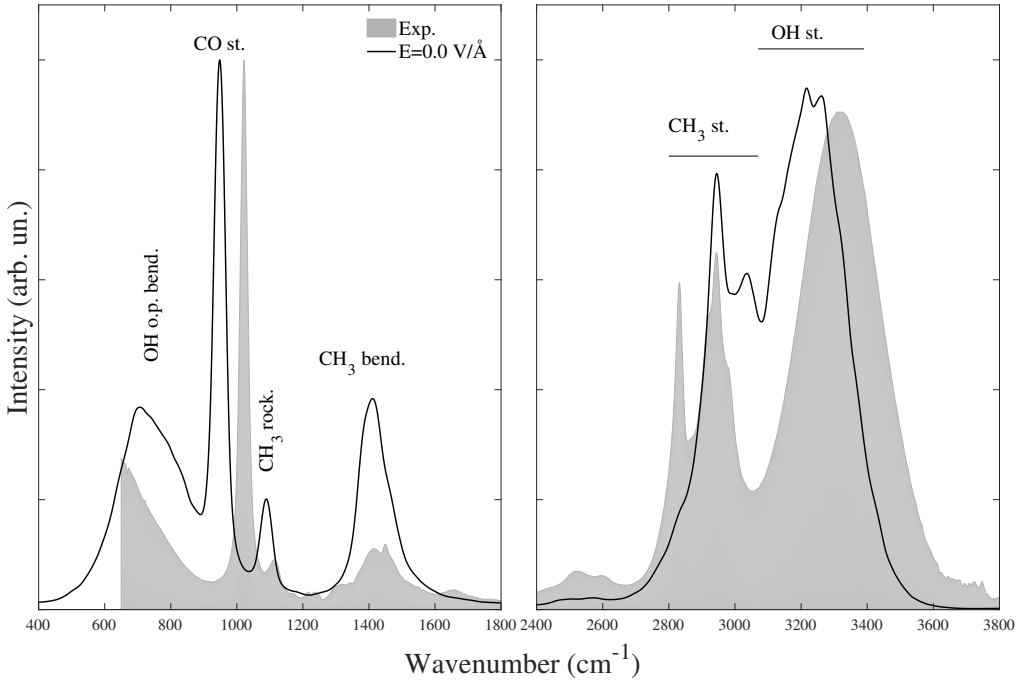

Figure 1. Infrared (IR) absorption spectra of liquid methanol determined from AIMD simulation (black line) at room temperature and in absence of electric field. The experimental results [76] are shown as gray shading for reference. In the two panels, the intensities of the highest peaks are rigidly scaled for better comparison between computations and experiment.

One of the key features emerging from IR spectra of H-bonded systems is represented by the possibility of monitoring the effects induced by variations of external thermodynamic parameters such as temperature, pressure, or electric field. When a static and homogeneous electric field is applied in neat liquid methanol, a contraction of the entire

IR spectrum is recorded, as shown in Figure 2. In fact, whereas low-frequency modes are blue-shifted, high-frequency modes are sizably red-shifted by the electric field. Moreover, such a phenomenon, known as the vibrational Stark effect [44,45], is progressive with respect to the increment of the field strength, as it is visible in the spectra emerging from AIMD simulations carried out at several field intensities and displayed in Figure 2. This field-induced effect is fully stackable with that observed in liquid water upon exposure to static external electric fields [47], indicating that the collective vibrational response of polar liquids to externally applied electrostatic potential gradients exhibits some common features. However, whereas in bulk water the peak's height and, to some extent, also the full-width at half-maximum (FWHM) of the OH-stretching band are not altered by the field [47], in liquid methanol they change significantly upon field exposure. In fact, the height of the peak of the OH-stretching band progressively decreases with the increase in the field intensity, as shown in Figure 2. More complicated is the interpretation of the effects of the field on the FWHM of the OH-stretching band because of the combined effect carried by the red-shift imposed by the field and the presence of the closely-located—at lower frequencies—CH_3-stretching band. The field-induced red-shift of the OH-stretching band leads, indeed, to a partial mixing of the typical vibrational frequencies of this mode with those of the CH_3 stretching. In this way, the application of intense electric fields (i.e., $E \geq 0.25$ V/Å) disrupts the separation of those bands in the IR spectrum of liquid methanol, as shown by the blue and violet curves in Figure 2 at frequencies around $\sim$3000 cm^{-1}.

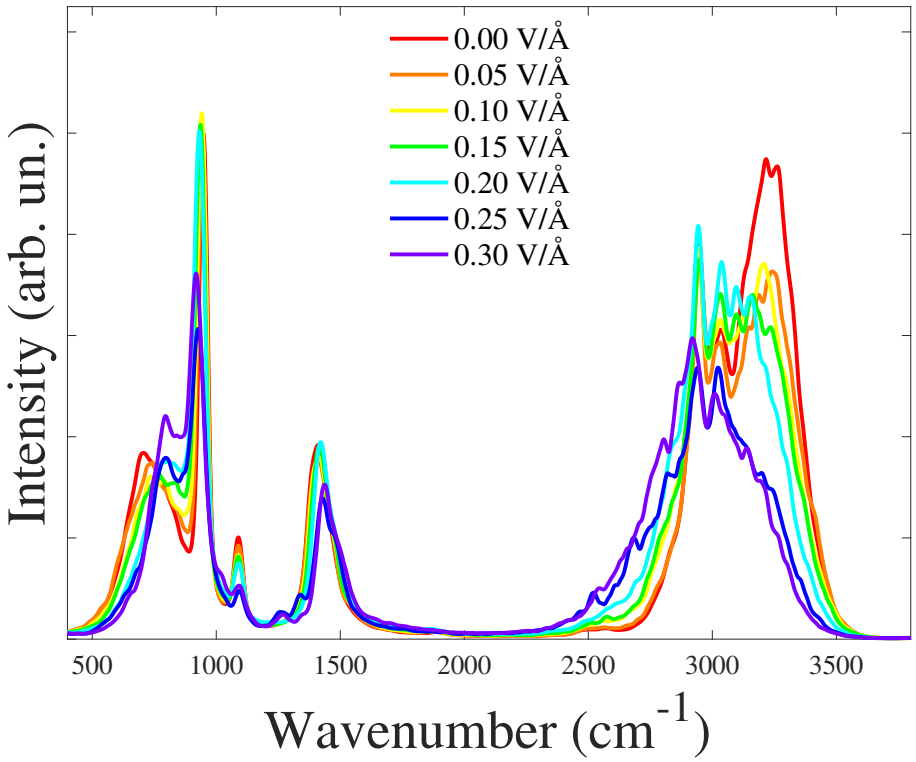

Figure 2. IR absorption spectra of bulk liquid methanol determined in absence (red line) and under different field intensities (colored from orange to violet) as detailed in the legend at 300 K.

Although the CH_3-bending mode—whose frequencies of vibration fall at $\sim$1400 cm^{-1}—appears to be less affected by the application of the field, a slight but visible blue-shift accompanied by an intensity reduction is recorded at the highest field intensities here explored, as shown in Figure 2. Whereas no appreciable field-induced frequency shifts are exhibited by the CH_3-rocking band, the height of the respective peak decreases as the intensity of the field is increased, as shown in Figure 2. At lower frequencies, although a slight red-shift is observed, the very narrow CO-stretching band is only weakly altered by the field up to strengths equal to 0.25 V/Å, a threshold marking an abrupt decrease

in the intensity of such a band. At the same time, the out-of-plane OH-bending band is progressively blue-shifted as the field strength is increased and the height of its peak increases as well from $E = 0.25$ V/Å. Thus, the application of static electric fields sensibly modifies the vibrational features of bulk liquid methanol. Furthermore, starting from field intensities equal to 0.25 V/Å, an abrupt change of several IR bands is recorded, indicating the onset of structurally important modifications at the molecular level.

Methanol IR spectra for different temperatures are shown in Figure 3. Despite a physiologic increase of the intensity of some bands accompanied by a slight narrowing of the allowed frequencies of vibration (i.e., the OH-stretching, the CH_3-stretching, the CH_3-bending, and the out-of-plane OH-bending bands), no systematic shift in the average frequency of vibration is recorded upon decreasing the external temperature, with only one exception; in fact, the frequencies of the out-of-plane OH-bending mode of vibration undergo a slight increase upon decreasing the temperature, as shown in the low-frequency region of Figure 3, a trend which coincides with that induced by an increment of the strength of an external electric field. However, differently from what is observed in liquid water, where the application of a static electric field leads to a more "ice-like" structured liquid [47], in neat liquid methanol the effects induced by the field are definitely separated from those induced by a decrease in the temperature. Generally speaking, the features induced by the application of a vector (i.e., the oriented electric field) and those afforded by varying a scalar quantity (i.e., the temperature) on matter are by their own nature a priori deeply different. Thus, the higher multiplicity of the H-bond network present in liquid water—where each molecule is on average involved in ∼4 H-bonds—with respect to that of methanol—where each molecule is on average involved in only ∼2 H-bonds—significantly mitigates the differences carried by an electric field increase and a temperature decrease. In fact, whereas in water the direction imposed by the external field to the dipole vectors can lead to H-bonded solid-like structures, in methanol it can only lead to linear chains of H-bonded molecules all oriented along the field axis and with the hydrophilic heads placed in favor of the field [49,50], a circumstance preventing the formation of any methanol solid phase [79]. This way, whilst electrofreezing may in principle be possible in water, as suggested in the literature [46–48], it appears to be unlikely in methanol. In fact, as also shown in Table 1, the seminal effect produced by the external field is that of decreasing the average number of H-bonds $<n_{HB}>$—as determined from geometric criteria [20,23]—in which a methanol molecule is statistically involved. Nevertheless, once a fraction of molecules has been re-oriented by the field [49], a slight increase in the number of H-bonds is recorded, even though it is up to values significantly smaller than those observed in absence of the field, as reported in Table 1. Beyond 0.30 V/Å, some molecular dissociations occur, leading to correlated proton-transfer events [49]. Although proton transfer takes place across the H-bond network, the average lifetime of H-bonds in liquid methanol decreases for field intensities higher than those explored in the current investigation (i.e., above 0.30 V/Å) [49].

Modifications induced to the IR spectrum by the application of an oriented external static and homogeneous electric field (Figure 2) take their roots in the interactions established by the external electrostatic potential gradient and the molecular methanol dipoles. As shown in Figure 4, where the molecular dipole moment magnitude is plotted as a function of the field strength, the averaged (over the duration of the AIMD simulations and the number of molecules composing the simulation boxes) methanol dipole moment linearly increases with increasing the strength of the externally applied field. Such a finding is perfectly stackable with that observed in liquid water as well [47].

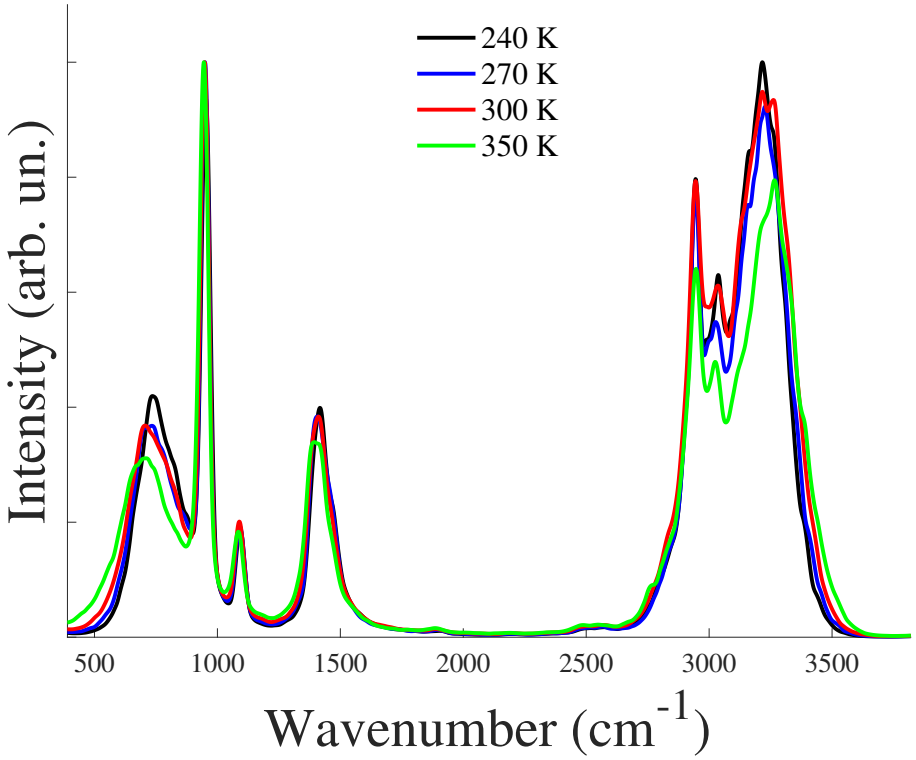

Figure 3. IR absorption spectra of bulk liquid methanol determined at 240 K (black line), 270 K (blue line), 300 K (red line), and 350 K (green line) in absence of electric field. Notice that the red-line curve coincides with the red-line curve of Figure 2 and with the black-line curve of Figure 1 (i.e., $T = 300$ K and $E = 0.00$ V/Å).

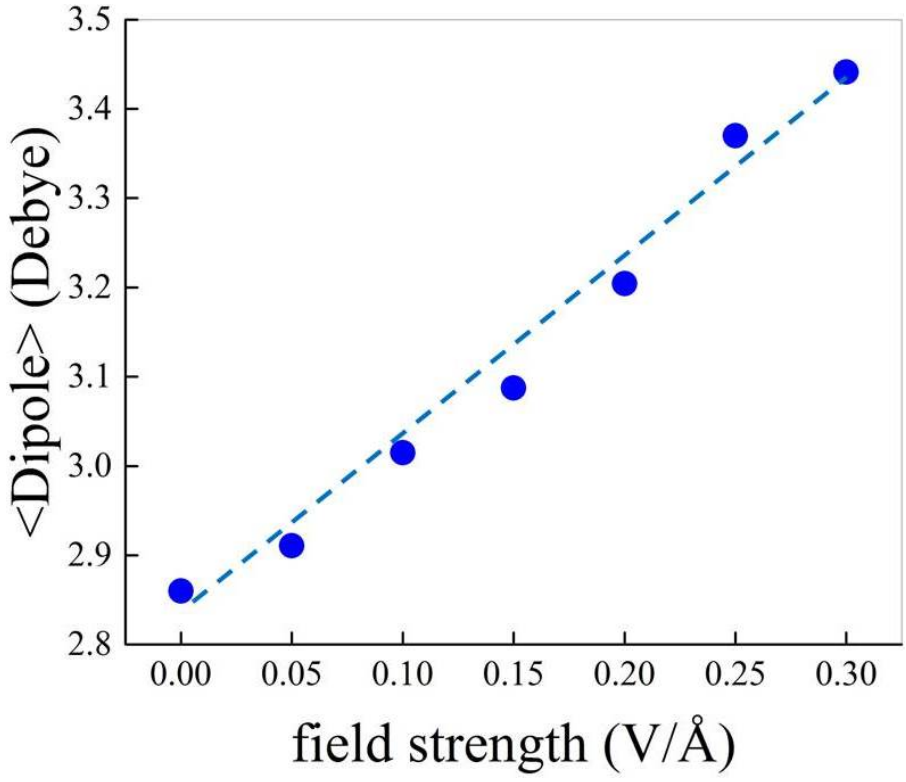

Figure 4. Average molecular dipole moment magnitude as a function of the field strength. Calculated points are plotted as full blue circles whereas the linear fit is presented as dashed blue line.

Table 1. Average number of H-bonds per molecule at different field strengths.

E Field (V/Å)	$<n_{HB}>$
0.00	2.04
0.05	1.72
0.10	1.43
0.15	1.49
0.20	1.50
0.25	1.57
0.30	1.63

Methanol dipole moments are intimately connected with the behavior of the OH and CO covalent bonds. As for the OH covalent bond, instead of monitoring the distributions of the lengths of such a bond, another very useful quantity has been evaluated. In fact, an indicator capable of monitoring the dissociation degree in H-bonded systems is the proton-sharing coordinate [80,81]. This latter is defined as $\delta = dOH - dO'H$, where dOH is the OH covalent bond length of a reference molecule, whereas $dO'H$ represents the length of the H-bond(s) that the reference molecule donates, as depicted in the inset of Figure 5b. When the proton is transiently closer to the acceptor than to the donor oxygen, then $\delta > 0$. Figure 5 shows the probability distributions of δ in bulk liquid methanol simulated by means of AIMD as a function of the field strength. For the sake of clarity, such a proton transfer coordinate has been restricted, during the post-processing analysis, in the region where the probability of finding a proton on a H-bond is maximum (i.e., $\delta \geq -0.8$). Moreover, since we are interested in evaluating eventual (partial) proton transfer events, the behavior of the distributions for $\delta \to 0$ is highlighted by its logarithmic plot (Figure 5b). The range of field strengths here explored is not capable of dissociating statistically significant amounts of methanol molecules, as shown by the tails of the curves in Figure 5b and as also indicated elsewhere [50]. However, the application of intense static electric fields induces a sizable increase in the "proton excursion" events along the H-bonds, in that OH covalent bonds appear weakened by the field and hydrogen atoms get closer to the oxygen atom of the neighboring H-bonded methanol molecule when the field is increased, as shown in Figure 5a,b. Such evidence is sufficient to give a rationale to the observed field-induced red-shift of the OH-stretching band of the IR spectrum of Figure 2.

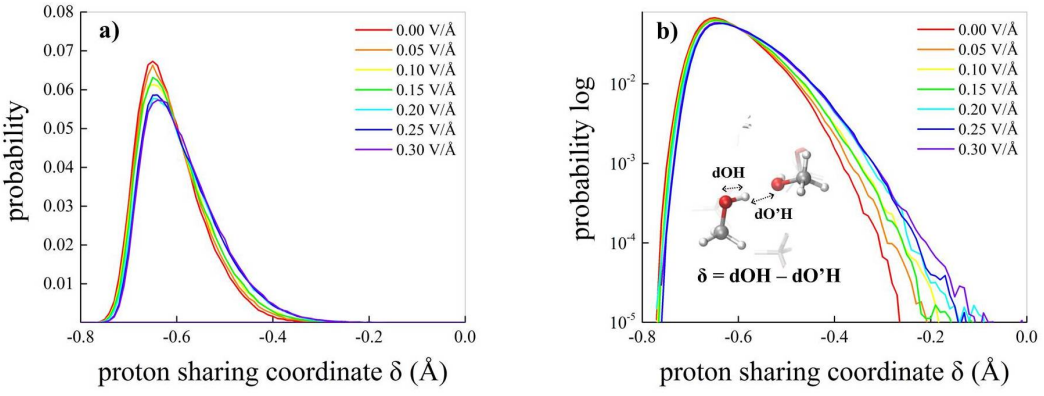

Figure 5. Probability distributions of the proton-sharing coordinate δ between methanol molecules under linear (**a**) and logarithmic (**b**) plots at different electric field strengths as detailed in the legends. In the inset of (**b**), the definition of the coordinate, which is determined for every hydrogen atom in the system involved in a tight H-bond, is shown.

Similarly to the OH bond, the CO covalent bond is also elongated by the field, as shown in Figure 6a. In particular, the maximum of the distribution of this intramolecular length shifts toward larger values as the field intensity is increased, indicating that

methanol molecules are stretched by the application of the field. Thus, the field not only re-orients progressively larger portions of molecules toward its direction [49], but also sizably stretches methanol covalent bonds, a circumstance dramatically enhancing the chemical reactivity of the sample. It is worth noting that such an effect is not affordable with the mere variation in the external temperature, as shown in Figure 6b, where the CO bond length distributions at different temperatures and in the absence of the field are plotted.

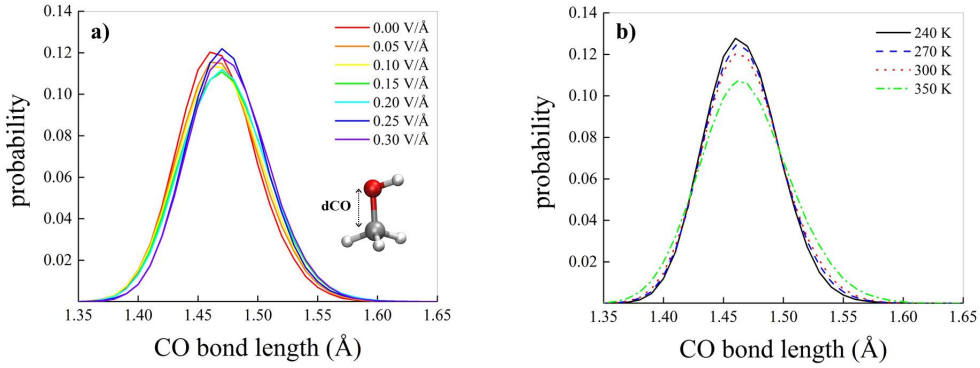

Figure 6. Distributions of the lengths of the CO covalent bonds in bulk liquid methanol determined for different field strengths at room temperature (**a**) and in the absence of the external field for diverse temperatures (**b**).

Such qualitative behavior of the CO bond length distributions, determined either under the field action or under different temperatures, is quantitatively examined in Figure 7. In particular, Figure 7a shows the average CO bond length as a function of the field strength and, in the inset, the same quantity is plotted against the temperature. Whereas the application of the field—along with its polarization effects—progressively stretches the CO bond of the methanol molecules, this latter length is somehow insensitive to the increase/decrease in the temperature of the sample. Such evidence clearly explains not only the observed field-induced red-shift of the CO-stretching band of the IR spectrum shown in Figure 2, but also the independence (at least in the range of the explored temperatures) of the same band upon varying the temperature of the liquid (Figure 3). Furthermore, whilst a temperature increase progressively broadens the CO length distribution (inset of Figure 7b), a re-entrant effect is recorded when the electric field is applied. In fact, the FWHM of the CO bond length distribution is initially widened by the field, indicating that some methanol molecules start to explore longer CO bond lengths. However, when large portions of molecules are aligned and stretched by the field, they exhibit a smaller range of (larger) CO bond lengths, as shown in Figure 7b.

General effects induced either by the electric field or by the temperature on the molecular structure of bulk liquid methanol can be evaluated by means of the relevant atomistic radial distribution functions (RDFs) plotted in Figure 8. The application of an external electric field does not sizably alter the typical local structure of the first-neighboring molecules. In fact, as shown in the top panel of Figure 8 (left), neither the height nor the location of the first peak of the OO RDF are modified by the field. However, the second peak of the OO RDF moves toward shorter distances indicating that the second solvation shell is slightly compressed as the field intensity is progressively increased. As far as temperature effects on the OO RDF are concerned (Figure 8, top panel on the right), the situation is completely different. In fact, whereas the location of all peaks and dips is not affected by the temperature variation, the height of all peaks (dips) decreases (increases), manifestly indicating the de-structuring process of the H-bond network triggered by a rise in the temperature (Figure 8, top panel on the right). Similar conclusions earned from the OO RDFs can also be extracted from the intermolecular OH RDFs plotted in the central panel of Figure 8. Finally, the analysis conducted for the CO bond length is also

partially manifested from the intermolecular CO RDFs presented in the bottom panel of Figure 8. In fact, whereas the first peak of the CO RDF moves toward larger distances upon increasing the field intensity (Figure 8, bottom panel on the left), as a consequence of the field-induced molecular alignment and stretching, only a broadening and a general decrease (increase) of the peaks (dips) is observed in the CO RDFs determined for different temperatures (Figure 8, bottom panel on the right). These findings, gathered from direct atomistic evidence, magnify once again the differences observed in the vibrational response of bulk liquid methanol to the application of either an external electric field or upon varying the temperature in the absence of the field.

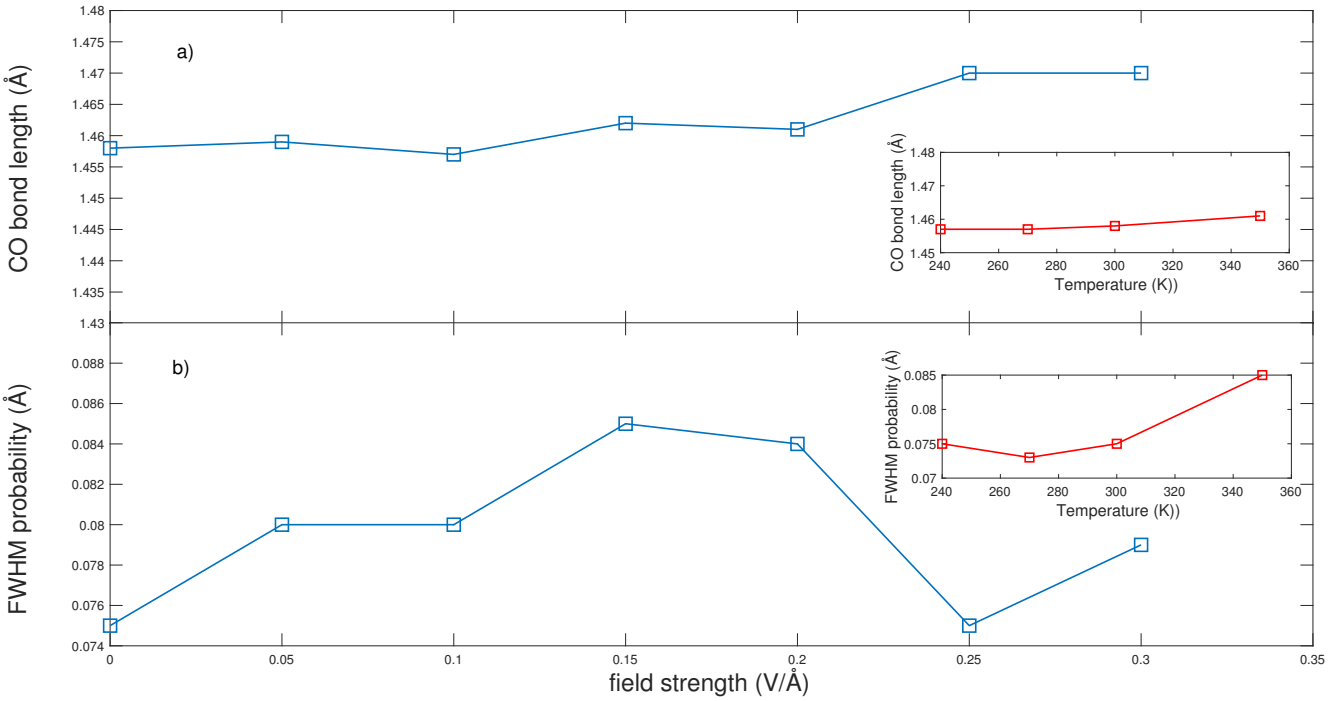

Figure 7. Average CO covalent bond length (**a**) and full-width at half-maximum probability of the CO covalent bond length distribution (**b**) determined as a function of the field strength. In the insets, the same quantities are determined for the zero-field case and as a function of the temperature.

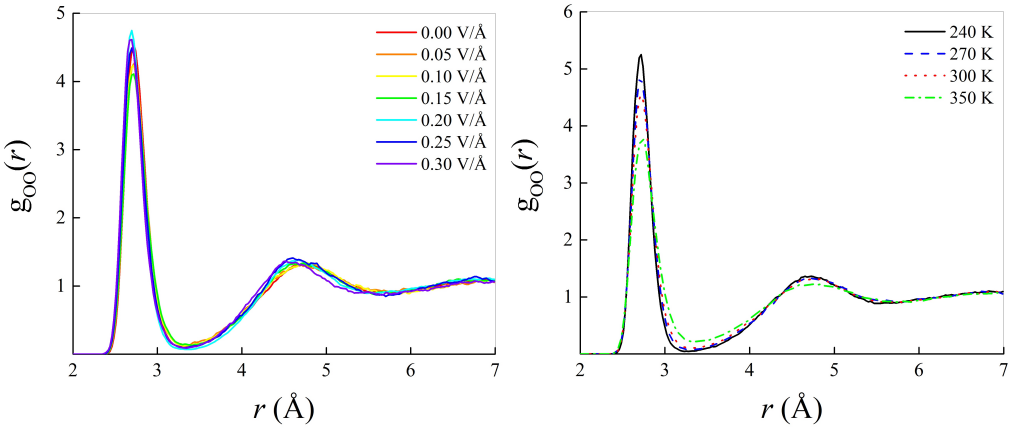

Figure 8. *Cont.*

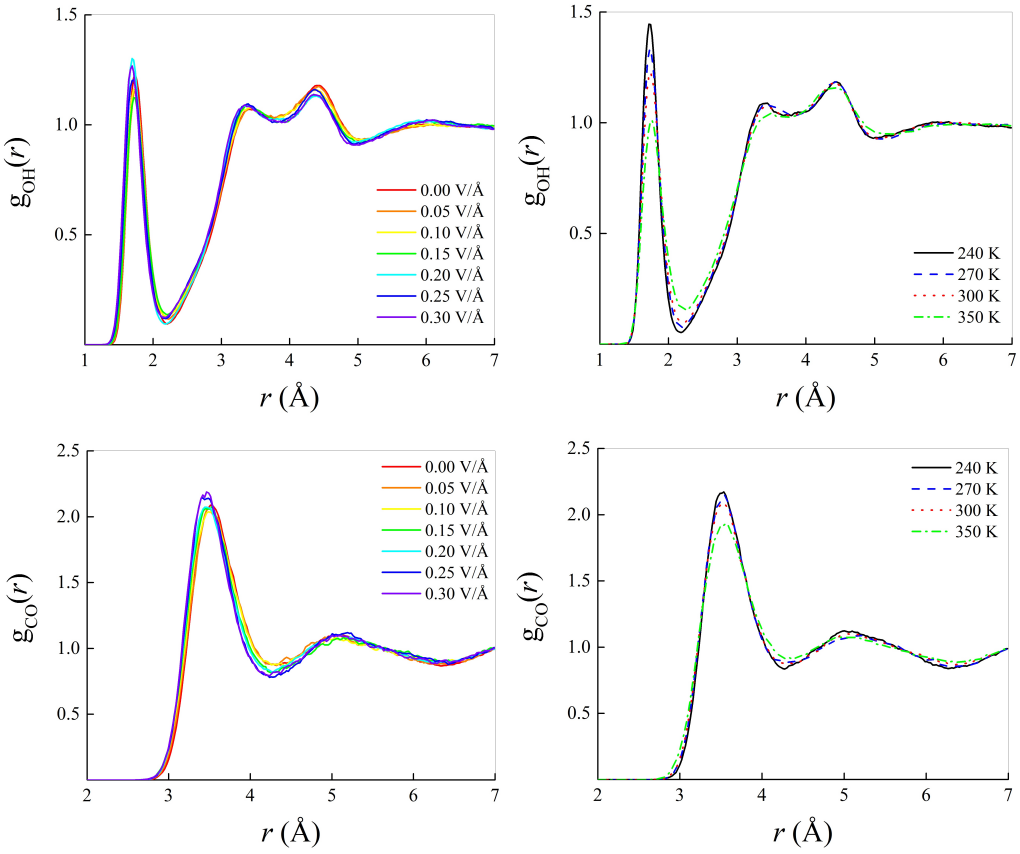

Figure 8. Intermolecular oxygen–oxygen (**top**), oxygen–hydrogen (**center**), and carbon–oxygen (**bottom**) radial distribution functions (RDFs) in bulk neat methanol at different field strengths and at room temperature (**left**) and in the zero-field case and for different values of the temperature (**right**).

4. Conclusions

In the current study, by employing state-of-the-art ab initio molecular dynamics (AIMD) simulations, we have reported the IR spectra of liquid methanol under the action of static and homogeneous electric fields with intensities up to 0.30 V/Å. Moreover, with the aim of comparing electric-field-induced and temperature-induced effects, we have here also presented IR spectra of liquid methanol at different temperatures, from 240 K up to 350 K. Although some electric-field-induced effects resemble the response of other polar liquids (such as the global contraction of the IR spectrum upon field exposure), it turned out that, contrarily to water, the "electrofreezing" phenomenon is unlikely to happen in liquid methanol. Differently from what is observed in liquid water, where the application of a static electric field leads to a more "ice-like" structured liquid [47], in neat liquid methanol the effects induced by the field are sharply separated from those produced by a decrease in the temperature.

The effects produced by the application of a vector (i.e., the oriented electric field) and those afforded by varying a scalar quantity (i.e., the temperature) on matter are, a priori and by their own nature, deeply different. However, the higher multiplicity and larger percolation degree of the H-bond network present in liquid water with respect to that of methanol significantly mitigates the intrinsic differences carried by an electric field intensity increase and a temperature decrease. In fact, whereas in water the direction imposed by the external field to the dipole vectors can lead to H-bonded solid-like structures, in methanol it can only lead to linear chains of H-bonded molecules all oriented along the field axis and with the hydrophilic heads placed in favor of the field [49,50], a circumstance preventing the formation of any methanol solid phase. Moreover, here we have shown that the seminal effect produced by the external field is that of decreasing the average

number of H-bonds in which a methanol molecule is statistically involved. Additionally to the evidence visible at the atomistic level, the different response of liquid methanol to diverse external thermodynamic variables (electric field and temperature) is manifested from the completely different vibrational response this liquid exhibits in the IR spectra here presented. This way, whilst the electrofreezing phenomenon appears to be possible in water in principle, it is unlikely in methanol.

Author Contributions: Conceptualization, G.C.; methodology, G.C.; software, G.C.; validation, G.C., S.T. and F.S.; formal analysis, G.C., S.T. and F.S.; investigation, G.C., S.T. and F.S.; resources, J.S.; data curation, G.C. and S.T.; writing—original draft preparation, G.C., S.T. and F.S.; writing—review and editing, G.C., S.T. and F.S. All authors have read and agreed to the published version of the manuscript.

Funding: This research received no external funding.

Institutional Review Board Statement: Not applicable.

Informed Consent Statement: Not applicable.

Data Availability Statement: Trajectories, MLWF center files, and all data are available upon reasonable request to the authors.

Conflicts of Interest: The authors declare no conflict of interest.

References

1. Pauling, L. *The Nature of the Chemical Bond*; Cornell University Press: Ithaca, NY, USA, 1960.
2. Angell, C.A. *Hydrogen Bonded Liquids*; Dore, J.C., Texeira, J., Eds.; Kluwer Academic: Dordrecht, The Netherlands, 1991.
3. Chang, C.D. Hydrocarbons from methanol. *Catal. Rev. Sci. Eng.* **1983**, *25*, 1–118. [CrossRef]
4. Tian, P.; Wei, Y.; Ye, M.; Liu, Z. Methanol to olefins (MTO): From fundamentals to commercialization. *ACS Catal.* **2015**, *5*, 1922–1939. [CrossRef]
5. De Wild, P.J.; Verhaak, M.J.F.M. Catalytic production of hydrogen from methanol. *Catal. Today* **2000**, *60*, 3–10. [CrossRef]
6. Dahl, I.M.; Kolboe, S. On the reaction mechanism for hydrocarbon formation from methanol over SAPO-34: I. Isotopic labeling studies of the co-reaction of ethene and methanol. *J. Catal.* **1994**, *149*, 458–464. [CrossRef]
7. Xu, M.; Lunsford, J.H.; Goodman, D.W.; Battacharyya, A. Synthesis of dimethyl ether (DME) from methanol over solid-acid catalysts. *Appl. Catal. A Gen.* **1997**, *149*, 289–301. [CrossRef]
8. Li, W.; Pan, C.; Zhang, Q.; Liu, Z.; Peng, J.; Chen, P.; Lou, H. Upgrading of low-boiling fraction of bio-oil in supercritical methanol and reaction network. *Bioresour. Tech.* **2011**, *102*, 4884–4889. [CrossRef] [PubMed]
9. Olah, G.A.; Goeppert, A.; Prakash, G.K.S. *Beyond Oil and Gas: The Methanol Economy*; 2nd Updated and Enlarged Edition; Wiley-VCH: Winheim, Germany, 2009.
10. Yamaguchi, T.; Hidaka, K.; Soper, A.K. The structure of liquid methanol revisited: A neutron diffraction experiment at −80°C and +25°C. *Mol. Phys.* **1999**, *97*, 603–605; Erratum in 1999, *97*, 603–605. [CrossRef]
11. Weitkamp, T.; Neuefeind, J.; Fischer, H.E.; Zeidler, M.D. Hydrogen bonding in liquid methanol at ambient conditions and at high pressure. *Mol. Phys.* **2000**, *98*, 125. [CrossRef]
12. Boyd, S.L.; Boyd, R.J. A Density Functional Study of Methanol Clusters. *J. Chem. Theory Comput.* **2007**, *3*, 54. [CrossRef]
13. Sum, A.K.; Sandler, S.I. Ab Initio Calculations of Cooperativity Effects on Clusters of Methanol, Ethanol, 1-Propanol, and Methanethiol. *J. Phys. Chem. A* **2000**, *104*, 1121. [CrossRef]
14. Sarkar S.; Joarder, R.N. Molecular clusters and correlations in liquid methanol at room temperature. *J. Chem. Phys.* **1993**, *99*, 2032. [CrossRef]
15. Montague, D.G.; Gibson, I.B.; Dore, J.C. Structural studies of liquid alcohols by neutron diffraction: I. Deuterated methyl alcohol CD3OD. *Mol. Phys.* **1981**, *44*, 1355. [CrossRef]
16. Narten, A.H.; Habenschuss, A. Hydrogen bonding in liquid methanol and ethanol determined by x-ray diffraction. *J. Chem. Phys.* **1984**, *80*, 3387. [CrossRef]
17. Magini, M.; Paschina, G.; Piccaluga, G. On the structure of methyl alcohol at roomtemperature. *J. Chem. Phys.* **1982**, *77*, 2051. [CrossRef]
18. Wilson, K.R.; Cavalleri, M.; Rude, B.S.; Shaller, R.D.; Catalano, T.; Nilsson, A.; Saykally, R.J.; Pettersson, L.G. X-ray Absorption Spectroscopy of Liquid Methanol Microjets: Bulk Electronic Structure and Hydrogen Bonding Network. *J. Phys. Chem. B* **2005**, *109*, 10194. [CrossRef]
19. Jorgensen, W.L. Quantum and statistical mechanical studies of liquids. 11. Transferable intermolecular potential functions. Application to liquid methanol including internal rotation. *J. Am. Chem. Soc.* **1981**, *103*, 341. [CrossRef]
20. Haughney, M.; Ferrario, M.; McDonald, I.R. Molecular-dynamics simulation of liquid methanol. *J. Phys. Chem.* **1987**, *91*, 4934. [CrossRef]

21. Handgraaf, J.W.; van Erp, T.S.; Mejer, E. Ab initio molecular dynamics study of liquid methanol. *J. Chem. Phys. Lett.* **2003**, *367*, 617. [CrossRef]
22. Morrone, J.A.; Tuckerman, M.E. Ab initio molecular dynamics study of proton mobility in liquid methanol. *J. Chem. Phys.* **2002**, *117*, 4403. [CrossRef]
23. Pagliai, M.; Cardini, G.; Righini, R.; Schettino, V. Hydrogen bond dynamics in liquid methanol. *J. Chem. Phys.* **2003**, *119*, 6655. [CrossRef]
24. Shaik, S.; de Visser, S.P.; Kumar, D. External Electric Field Will Control the Selectivity of Enzymatic-Like Bond Activations. *J. Am. Chem. Soc.* **2004**, *126*, 11746. [CrossRef]
25. Meir, R.; Chen, H.; Lai, W.; Shaik, S. Oriented Electric Fields Accelerate Diels-Alder Reactions and Control the Endo/Exo Selectivity. *ChemPhysChem* **2010**, *11*, 301. [CrossRef]
26. Suresh, S.J.; Prabu, A.L.; Arora, A. Influence of electric field on the hydrogen bond network of methanol. *J. Chem. Phys.* **2007**, *126*, 134502. [CrossRef]
27. Rai, D.; Kulkarni, A.D.; Gejji, S.P.; Pathak, R.K. Methanol clusters (CH3OH)n, n = 3–6 in external electric fields: Density functional theory approach. *J. Chem. Phys.* **2011**, *135*, 024307. [CrossRef] [PubMed]
28. Boda, M.; Patwari, G.N. Internal electric fields in methanol [MeOH]2–6 clusters. *Phys. Chem. Chem. Phys.*, **2020**, *22*, 10917–10923. [CrossRef] [PubMed]
29. Zhang, S.; Chen, W.; Shi, H.; Zhou, W.; Zhang, J. Theoretical Studies of the Influence of an Intermolecular Force and an Electric Field on the Methanol Raman Spectrum. *J. Phys. Chem. C*, **2020**, *124*, 6955–6963. [CrossRef]
30. Sellner, B.; Valiev, M.; Kathmann, S.H. Charge and electric field fluctuations in aqueous NaCl electrolytes. *J. Phys. Chem. B* **2013**, *117*, 10869–10882. [CrossRef] [PubMed]
31. Laage, D.; Elsaesser, T; Hynes, J.T. Perspective: Structure and ultrafast dynamics of biomolecular hydration shells. *Struct. Dyn.* **2017**, *4*, 044018. [CrossRef] [PubMed]
32. Saitta, A. M.; Saija, F.; Giaquinta, P. V. Ab Initio Molecular Dynamics Study of Dissociation of Water under an Electric Field. *Phys. Rev. Lett.* **2012**, *108*, 207801. [CrossRef]
33. Cassone, G. Nuclear Quantum Effects Largely Influence Molecular Dissociation and Proton Transfer in Liquid Water under an Electric Field. *J. Phys. Chem. Lett.* **2020**, *11*, 8983–8988. [CrossRef] [PubMed]
34. English, N.J.; Waldron, C.J. Perspectives on External Electric Fields in Molecular Simulation: Progress, Prospects and Challenges. *Phys. Chem. Chem. Phys.* **2015**, *17*, 12407–12440. [CrossRef] [PubMed]
35. Shafiei, M.; von Domaros, M.; Bratko, D.; Luzar, A. Anisotropic structure and dynamics of water under static electric fields. *J. Chem. Phys.* **2019**, *150*, 074505. [CrossRef] [PubMed]
36. Cassone, G.; Sofia, A.; Rinaldi, G.; Sponer, J. Catalyst-free hydrogen synthesis from liquid ethanol: An ab initio molecular dynamics study. *J. Phys. Chem. C* **2019**, *123*, 9202–9208. [CrossRef]
37. Petroff, C.A.; Cassone, G.; Sponer, J.; Hutchison, G.R. Intrinsically Polar Piezoelectric Self-Assembled Oligopeptide Monolayers. *Adv. Mater.* **2021**, 200748. [CrossRef]
38. Fried, S.D.; Boxer, S.G. Electric Fields and Enzyme Catalysis. *Annu. Rev. Biochem.* **2017**, *86*, 387–415. [CrossRef]
39. Murgida, D.H.; Hildebrandt, P. Electron-Transfer Processes of Cytochrome *c* at Interfaces. New Insights by Surface-Enhanced Resonance Raman Spectroscopy. *Acc. Chem. Res.* **2004**, *37*, 854–861. [CrossRef]
40. Sowlati-Hashjin, S.; Matta, C.F. The chemical bond in external electric fields: Energies, geometries, and vibrational Stark shifts of diatomic molecules. *J. Chem. Phys.* **2013**, *139*, 144101. [CrossRef]
41. Papanikolaou, P.; Karafiloglou, P. Investigating sigma bonds in an electric field from the Pauling's perspective: The behavior of Cl-X and H-X (X=C,Si) bonds. *Theor. Chem. Acc.* **2010**, *126*, 213–222. [CrossRef]
42. Rincon, L.; Mora, J.R.; Torres, F.J.; Almeida, R. On the activation of σ-bonds by electric fields: A Valence Bond perspective. *Chem. Phys.* **2016**, *477*, 1–7. [CrossRef]
43. Stark, J. Observation of the Separation of Spectral Lines by an Electric Field. *Nature* **1913**, *92*, 401. [CrossRef]
44. Bishop, D.M. The vibrational Stark effect. *J. Chem. Phys.* **1993**, *98*, 3179. [CrossRef]
45. Chattopadhyay, A.; Boxer, S.G. Vibrational Stark Effect Spectroscopy. *J. Am. Chem. Soc.* **1995**, *117*, 1449–1450. [CrossRef]
46. Svishchev, I.M.; Kusalik, P.G. Electrofreezing of Liquid Water: A Microscopic Perspective. *J. Am. Chem. Soc.* **1996**, *118*, 649–654. [CrossRef]
47. Cassone, G.; Sponer, J.; Trusso, S.; Saija, F. Ab initio spectroscopy of water under electric fields. *Phys. Chem. Chem. Phys.* **2019**, *21*, 21205–21212. [CrossRef]
48. Boyd, S.J.; Krishnan, Y.; Ghaani, M.R.; English, N.J. Influence of external static and alternating electric fields on self-diffusion of water from molecular dynamics. *J. Mol. Liq.* **2021**, *327*, 114788. [CrossRef]
49. Cassone, G.; Giaquinta, P.V.; Saija, F.; Saitta, A. M. Liquid methanol under a static electric field. *J. Chem. Phys.* **2015**, *142*, 054502. [CrossRef]
50. Cassone, G.; Sofia, A.; Sponer, J.; Saitta, A.M.; Saija, F. Ab Initio Molecular Dynamics Study of Methanol-Water Mixtures under External Electric Fields. *Molecules* **2020**, *25*, 3371. [CrossRef]
51. Hutter, J.; Iannuzzi, M.; Schiffmann, F.; VandeVondele, J. CP2K: Atomistic simulations of condensed matter systems. *Wiley Interdiscip. Rev.-Comput. Mol. Sci.* **2014**, *4*, 15. [CrossRef]

52. Vandevondele, J.; Krack, M.; Mohamed, F.; Parrinello, M.; Chassaing, T.; Hutter, J. QUICKSTEP: Fast and accurate Density Functional calculations using a mixed gaussian and plane waves approach. *Comput. Phys. Commun.* **2005**, *167*, 103. [CrossRef]
53. King-Smith, R.D.; Vanderbilt, D. Theory of polarization of crystalline solids. *Phys. Rev. B.* **1993**, *47*, 1651. [CrossRef]
54. Resta, R. Macroscopic polarization in crystalline dielectrics: The geometric phase approach. *Rev. Mod. Phys.* **1994**, *66*, 899. [CrossRef]
55. Berry, M.V. Quantal phase factors accompanying adiabatic changes. *Proc. R. Soc. Lond. A* **1984**, *392*, 45.
56. Umari, P.; Pasquarello, A. Ab initio molecular dynamics in a finite homogeneous electric field. *Phys. Rev. Lett.* **2002**, *89*, 157602. [CrossRef]
57. Cassone, G.; Pietrucci, F.; Saija, F.; Guyot, F.; Saitta, A.M. One-step electric-field driven methane and formaldehyde synthesis from liquid methanol. *Chem. Sci.*, **2017**, *8*, 2329–2336. [CrossRef]
58. Cassone, G.; Pietrucci, F.; Saija, F.; Guyot, F.; Sponer, J.E.; Sponer, J.; Saitta, A.M. Novel electrochemical route to cleaner fuel dimethyl ether. *Sci. Rep.* **2017**, *7*, 6901. [CrossRef]
59. Krack, M. Pseudopotentials for H to Kr optimized for gradient-corrected exchange-correlation functionals. *Theor. Chem. Acc.* **2005**, *114*, 145–152. [CrossRef]
60. Becke, A.D. Density-Functional exchange-energy approximation with correct asymptotic behavior. *Phys. Rev. A* **1988**, *38*, 3098. [CrossRef]
61. Lee, C.; Yang, W.; Parr, R.G. Development of the Colle-Salvetti correlation-energy formula into a functional of the electron density. *Phys. Rev. B* **1988**, *37*, 785. [CrossRef]
62. Grimme, S.; Antony, J.; Ehrlich, S.; Krieg, H. A consistent and accurate ab initio parametrization of Density Functional dispersion correction (DFT-D) for the 94 elements H-Pu. *J. Chem. Phys.* **2010**, *132*, 154104. [CrossRef]
63. Grimme, S.; Ehrlich, S.; Goerigk, L. Effect of the damping function in dispersion corrected Density Functional Theory. *J. Comp. Chem.* **2011**, *32*, 1456–1465. [CrossRef]
64. Lin, I.-C.; Seitsonen, A.P.; Tavernelli, I.; Rothlisberger, U. Structure and dynamics of liquid water from ab initio molecular dynamics—Comparison of BLYP, PBE, and revPBE Density Functionals with and without van der Waals corrections. *J. Chem. Theory Comput.* **2012**, *8*, 3902–3910. [CrossRef]
65. Bankura, A.; Karmakar, A.; Carnevale, V.; Chandra, A.; Klein, M.L. Structure, dynamics, and spectral diffusion of water from first-principles molecular dynamics. *J. Phys. Chem. C* **2014**, *118*, 29401–29411. [CrossRef]
66. Gillan, M.J.; Alfé, D.; Michaelides, A. Perspective: How good is DFT for water? *J. Chem. Phys.* **2016**, *144*, 130901. [CrossRef] [PubMed]
67. Habershon, S.; Fanourgakis, G.S.; Manolopoulos, D.E. Comparison of path integral molecular dynamics methods for the infrared absorption spectrum of liquid water. *J. Chem. Phys.* **2008**, *129*, 074501. [CrossRef]
68. Witt, A.; Ivanov, S.D.; Shiga, M.; Forbert, H.; Marx, D. On the applicability of centroid and ring polymer path integral molecular dynamics for vibrational spectroscopy. *J. Chem. Phys.* **2009**, *130*, 194510. [CrossRef]
69. Bussi, G.; Donadio, D.; Parrinello, M. Canonical sampling through velocity rescaling. *J. Chem. Phys.* **2007**, *126*, 014101. [CrossRef]
70. Brehm, M.; Kirchner, B. TRAVIS—A Free Analyzer and Visualizer for Monte Carlo and Molecular Dynamics Trajectories. *J. Chem. Inf. Model.* 2011, **51**, 2007–2023. [CrossRef]
71. Thomas, M.; Brehm, M.; Fligg, R.; Voehringer, P.; Kirchner, B. Computing vibrational spectra from ab initio molecular dynamics. *Phys. Chem. Chem. Phys.* **2013**, **15**, 6608–6622. [CrossRef]
72. Marzari, N.; Vanderbilt, D. Maximally localized generalized Wannier functions for composite energy bands. *Phys. Rev. B* **1997**, **56**, 12847–12865. [CrossRef]
73. Marzari, N.; Mostofi, A.A.; Yates, J.R.; Souza, I.; Vanderbilt, D. Maximally localized Wannier functions: Theory and applications. *Rev. Mod. Phys.* **2012**, **84**, 1419–1475. [CrossRef]
74. Neese, F. Prediction of molecular properties and molecular spectroscopy with density functional theory: From fundamental theory to exchange-coupling. *Coord. Chem. Rev.* **2009**, *253*, 526–563. [CrossRef]
75. Falk, M.; Whaley, E. Infrared spectra of methanol and deuteraded methanols in gas, liquid, and solid phases. *J. Chem. Phys.* **1961**, *34*, 1554. [CrossRef]
76. Doroshenck, I; Pogorelov, V.; Sablinskas, V. Infrared absorption spectra of monohydric alcohols *Dataset Pap. Chem.* **2013**, *2013*, 329406. [CrossRef]
77. Bertie, J.E.; Zhang, S.L.; Eysel, H.H.; Baluja, S.; Ahmed, M.K. Infrared intensities of Liquids XI: infrared refractive indices from 8000 to 2cm^{-1}, absolute integrated intensities, and dipole moment derivatives of methanol at 25°C. *Appl. Spectrosc.* **1993**, *47*, 1100. [CrossRef]
78. Ishiyama, T.; Sokolov, V.V.; Morita, A. Molecular dynamics simulation of liquid methanol. I. Molecular modeling including C–H vibration and fermi resonance. *J. Chem. Phys.* **2011**, *134*, 024509.
79. Lin, T.J.; Hsing, C.R.; Wei, C.M.; Kuo, J.L. Structure prediction of the solid forms of methanol: An ab initio random structure searching approach. *Phys. Chem. Chem. Phys.* **2016**, 18, 2736–2746 [CrossRef]
80. Marsalek, O.; Markland, T.E. Quantum dynamics and spectroscopy of ab initio liquid water: the interplay of nuclear and electronic quantum effects. *J. Phys. Chem. Lett.* **2017**, *8*, 1545–1551. [CrossRef]
81. Ceriotti, M.; Cuny, J.; Parrinello, M.; Manolopoulos, D.E. Nuclear quantum effects and hydrogen bond fluctuations in water. *Proc. Natl. Acad. Sci. USA* **2013**, *110*, 15591–15596. [CrossRef]